ChemComm
Chemical Communications

Accepted Manuscript

This article can be cited before page numbers have been issued, to do this please use: V. Abgarjan, A. Simonov, K. Kuk and M. Karg, *Chem. Commun.*, 2026, DOI: 10.1039/D6CC01855F.

ROYAL SOCIETY OF CHEMISTRY

rsc.li/chemcomm

View Article Online
DOI: 10.1039/D6CC01855F

Double-Anonymised Title Page

Title:

Dynamic structural evolution of soft colloidal monolayers under uniaxial compression

Authors:

Vahan Abgarjan,[a] Arkadiy Simonov,[b] Keumkyung Kuk,*[a,c] and Matthias Karg[a,d]

Affiliations:

[a]Institut für Physikalische Chemie I: Kolloide und Nanooptik, Heinrich-Heine-Universität Düsseldorf, Universitätsstr. 1, 40225 Düsseldorf, Germany

[b]Disordered Materials, Department of Materials, ETH Zürich, Vladimir-Prelog-Weg 5, 8093 Zürich, Switzerland

[c]Laboratory for Soft Materials and Interfaces, Department of Materials, ETH Zürich, Vladimir-Prelog-Weg 5, 8093 Zürich, Switzerland

[d]Physikalische Chemie funktionaler Polymere, Institut für Chemie, Martin-Luther-Universität Halle-Wittenberg, Von-Danckelmann-Platz 4, 06120 Halle (Saale), Germany

Acknowledgements:

A Part of the research has been funded by Deutsche Forschungsgemeinschaft (DFG, KA3880/6-1). **K.K.** acknowledges Prof. Lucio Isa (ETH Zürich) for a helpful discussion and for enabling fruitful collaboration with **A.S.**

Author contributions:

K.K.: conceptualization, writing (original draft). **M.K.**: supervision, funding acquisition. **V.A.**: methodology. **A.S.**: formal analysis. All authors contributed to the review and editing.

ChemComm

View Article Online
DOI: 10.1039/D6CC01855F

COMMUNICATION

Dynamic structural evolution of soft colloidal monolayers under uniaxial compression

Received 00th January 20xx,
Accepted 00th January 20xx

DOI: 10.1039/x0xx00000x

We use small-angle light scattering to monitor microgel assembly at air/water interfaces during Langmuir trough compression in real time. We observe a reversible 30° reorientation of the hexagonal lattice, mediated by a metastable rectangular phase. This behavior arises from the unique deformability of soft colloids under uniaxial confinement.

Studies of colloids at fluid interfaces holds significance across technical applications (e.g., emulsion stabilization,[1, 2] material engineering[3-5]) as well as fundamental research (e.g., self-assembly,[6-8] colloidal interactions[9, 10]). Langmuir troughs (LTs) are commonly used to fabricate 2D structured materials and investigate assembly and phase behaviors.[11-14] The typical approach involves adsorbing the colloids of interest at fluid interfaces followed by controlled lateral compression using two barriers (changeable length *l* and fixed width *w*, **Fig 1A**) after a certain equilibration time while measuring surface pressure, Π. During this compression process, soft and deformable colloids such as microgels exhibit a spectrum of interparticle distances, in contrast to their rigid counterparts. In addition, the potential for forming non-hexagonal self-assembled structures (due to the soft interaction potential,[15] e.g., core-shell (CS) structured microgels with hydrodynamic diameter, D_h, **Fig 1B**) has captured the interest of a broad scientific community and has been extensively explored in recent years.[11, 14]

Recent works brought attention to the importance of *in situ* monitoring of soft colloids during such interfacial assembly processes. Using small-angle light scattering (SALS)[16] and fluorescence microscopy combined with a LT,[17, 18] *in situ* microstructures were shown to differ from those obtained *ex situ* after Langmuir-Blodgett deposition, evidencing transfer-induced structural changes.[19] Furthermore, despite maintaining near-hexagonal order, uniaxial LT compression was found to induce anisotropy in the microstructure even at low speeds.[20] Similar findings were reported in different systems, evidenced by an orientation-dependent Π, e.g., silica nanoparticles,[21] carbon nanotubes,[22] poly(*N*-isopropylacrylamide) (PNIPAM) microgels,[23] and proteins.[24] This suggests deformation and relaxation colloid monolayers of during uniaxial compression is more intricate than previously assumed. To fill this knowledge gap, fast and non-invasive in situ measurements are required.

Here we move beyond near-equilibrium assembly and examine the dynamic, out-of-equilibrium lattice changes of soft colloidal monolayers at the air/water interface (deformed due to surface tension with diameter, D_i, at the interface, **Fig 1C**) during compression and expansion cycles using LT-SALS. This approach allows real-time structural monitoring over mm²-scale areas at higher compression and expansion speeds, information inaccessible to real-space microscopy.

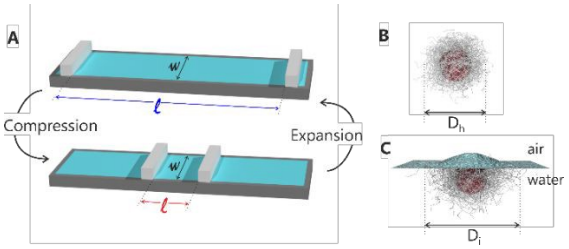

Figure 1. A) Uniaxial compression and expansion in a Langmuir trough, with length *l* and width *w*, at the air/water interface. **B**) CS microgel in bulk with a hydrodynamic diameter, D_h, and **C**) the same CS microgel absorbed at the air/water interface with an interfacial diameter, D_i. $D_i > D_h$ due to the lateral stretching of the microgel shell caused by the large interfacial tension.

Using seeded precipitation polymerization, we synthesized CS microgels with silica cores and soft, deformable PNIPAM shells. The cores had mean diameter of 340 nm measured by transmission electron microscopy (JEOL JEM-2100 Plus). We used a nominal crosslinker density of 5.2 mol.% for the shells. This resulted in microgels with overall hydrodynamic diameter, D_h of 791 nm (swollen state) measured by dynamic light scattering (Zetasizer Nano S, Malvern Panalytical). Detailed synthesis and purification protocols are described elsewhere.[25] The microgels in ethanol were spread onto the air/water interface in the Langmuir trough and left to equilibrate for at least 30 minutes. CS microgels are known to adsorb strongly to liquid interfaces.[14] Compression and expansion experiments were performed in a Langmuir trough (KSV NIMA, Biolin Scientific) equipped with a microscopy window in the bottom plate. Diffraction patterns were recorded by LT-SALS in real time. Setup

a.

View Article Online
DOI: 10.1039/D6QC01855F

specifications and measurement protocols are detailed elsewhere.[16, 20]

Fig 2 shows representative diffraction patterns from monolayers that self-assembled from monodisperse CS microgels during conventional uniaxial compression. The total reduction in interface area with a slow compression speed of 1 mm/min corresponds to 43% of the initial area. The captured diffraction patterns, initially in blue (I_{Laser} = 405 nm) on a dark background, were converted to grayscale and inverted using ImageJ.[26] Additionally, the patterns were rotated to align the compression direction horizontally for reasons of clarity and visibility. The diffraction patterns in **Fig 2A-D** show pronounced Bragg peaks with a six-fold symmetry that is related to the hexagonal packing (p6mm symmetry) of the CS microgels in the monolayer. The peaks shift to higher angles, i.e., the radial positions of the peak centers increase as Π increases (measured Πs: **A**) 23.2, **B**) 26.6, **C**) 27.6, and **D**) 29.6 mN/m), indicating that the interparticle distance decreases with compression (calculated assuming that the microstructure is hexagonally assembled and its strain is the same in all directions: **A**) 963 ± 76, **B**) 785 ± 75, **C**) 687 ± 52, and **D**) 600 ± 41 nm). At a closer look, the diffraction patterns become increasingly stretched along the compression direction with increasing compression, i.e. reduction in area. This anisotropy indicates that the interparticle distance along the compression axis decreases in real space relative to the orthogonal direction (width direction of the trough, *w*, as depicted in **Fig 1A**). In other words, the anisotropy of the microstructure caused by uniaxial compression becomes more pronounced as compression continues (aspect ratio, fitted with an ellipse: **A**) 1.06, **B**) 1.16, **C**) 1.16, and **D**) 1.15). The corresponding compression isotherm and interparticle distance as a function of surface pressure as well as normalized trough area, can be found in the **Supporting Information** (**SI**), in **Fig S1** and **Table S1**. For clarity, we will refer to samples with stretched six Bragg peaks as hexagonal lattices throughout this article if they retain six peaks, although strictly speaking they no longer exhibit six-fold rotational symmetry. For numerous microgel-assembled monolayers, the initial lattice orientation appears to be random. However, as compression proceeds, the lattice tends to reorient in such a way that two vertices of the hexagon in real space align with the compression direction. **Fig 2E** illustrates the relationship between the real and reciprocal lattice of a hexagonal structure in terms of lattice vectors and the angles between them. The blue circles represent the reciprocal lattice points (Bragg peaks) resembling the diffraction pattern captured in **Fig 2D**, while the red circles and vectors represent the corresponding real-space lattice.

This preference for lattice orientation, where the two opposite vertices of the hexagons in real space align with the compression direction, is somewhat counterintuitive, as simple geometric considerations would suggest that compression along the edges would allow for more efficient packing through particle sliding. However, the observed preference for vertex alignment suggests that non-linear effects and collective particle interactions dominate over simple packing considerations. **Fig 3** simulates vertex-vertex (**A-C**) and edge-edge compression (**D-F**) of the hexagon. Compression along the vertices causes the microgels at the vertices to come into contact with the central microgel earlier on ("hard direction") while leaving empty spaces between the rows of microgels. In contrast, compression along the edges (**D-E**) allows the two microgels at the ends of the edges to slide between the microgels in neighboring rows ("soft direction") and thus higher compression state. As compression proceeds in a soft direction, the microgel array undergoes a transitional phase before returning to hexagonal symmetry with its lattice orientation shifted by 30 degrees during the process. This behavior has not been observed in conventional Langmuir compression at low speeds, likely due to the relatively fast relaxation and rearrangement of microgels under such conditions. When the compression speed is high, the strain experienced by the microgel monolayer is likely to become more pronounced per unit time, while relaxation occurs relatively slowly. These dynamic rearrangements of the colloidal system may provide intriguing insights into properties such as interparticle potential and metastable transition states.[27] Additionally, they can reveal interesting metastable phases, aided by the slower kinetics of colloids compared to their atomic counterparts. In the following, we explore this far-from-equilibrium behavior of soft colloidal monolayers under compression and expansion.

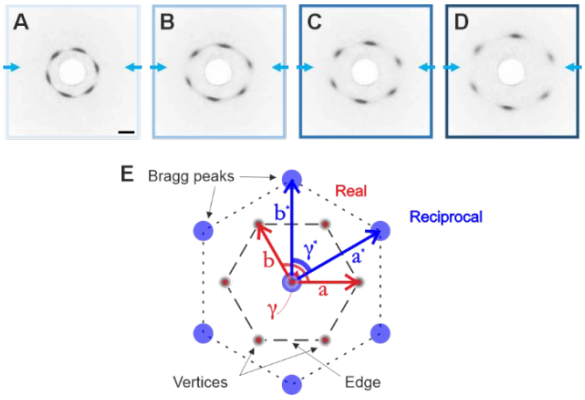

Figure 2. Compression of CS monolayer and the diffraction patterns captured during the slow conventional compression at measured Π **A**) 23.2, **B**) 26.6, **C**) 27.6, and **D**) 29.6 mN/m. The blue arrows illustrate the compression direction. The scale bar corresponds to 10 mm. **E**) Real space hexagonal lattice vectors *a*, *b* and the angle, *γ*, between the two vectors (red) along with the corresponding reciprocal lattice and the vectors a^* and b^* and angle, γ^* (blue).

Here it is important to highlight that in slow uniaxial compression, it is generally assumed that the locally measured Π represents the overall compression state of the microgel monolayer at the time of measurement. However, when the barriers move quickly, this assumption breaks down. A high compression speed could lead to more uneven stress distribution, anisotropic strain, and the development of a local structural gradient,[20, 22, 28] one must therefore be cautious when comparing Π measured at different and/or high speeds (see **Fig. S2** for slow vs. fast interparticle distance hysteresis). **Fig 4** shows a rapid expansion-compression cycle of the pre-assembled CS monolayer recorded via LT-SALS at 27 mm/min compression speed. The full **Video S1** of this rapid expansion-compression cycle can be viewed in **SI**. The diffraction pattern in **Fig 4A** shows the microgel monolayer from **Fig 2D** after being further compressed to Π of 30 mN/m, reducing the trough area from 43 % to 31 %. The system was then allowed to equilibrate for 30 minutes before structural investigation. After the equilibration time, the calculated interparticle distance remains at 607 ± 20 nm, comparable

to the situation in **Fig 2D** (600 ± 41 nm) despite further reducing the area, indicating that the microgels relax over time. The microstructure relaxation, accompanied by an increase in interparticle distance, becomes more evident when the monolayer is subjected to perturbation, such as in oscillating barrier experiments, where the two barriers oscillate sinusoidally around a target position. This relaxation behavior of the microgel monolayer can be observed in V**ideo S2**, captured during an oscillating barrier experiment (frequency 200 mHz, area change relative to the starting area 2%). Further evidence of this relaxation is the accompanying change in the aspect ratio of the diffraction pattern, which decreases from 1.15 in **Fig 2D** to 1.02 in **Fig 4A**.

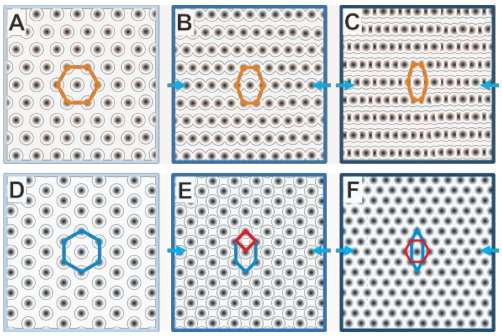

Figure 3. Simulated vertex-vertex (**A**-**C**) and edge-edge compression (**D**-**F**) for a hexagonal lattice of microgels. **A**-**C**) Under vertex-vertex compression, the microgels at the vertices meet the central microgel, making it a "hard direction" compression, while leaving empty spaces between rows. **D**-**F**) Under edge-edge compression, the microgels at the ends of the edges slide between neighboring rows of microgels, hence a "soft direction" compression.

Fig 4B-D show the evolution of the diffraction pattern during the rapid expansion at a barrier speed of 27 mm/min, which features a smooth, near 30° rotation of the Bragg peaks, with a pair of peaks eventually aligning with the compression direction. This indicates that the lattice orientation of the monolayer at the measuring point (at the center of the trough) rotates from a “hard” to a “soft direction” as the monolayer expands. Additionally, the pattern becomes elongated perpendicular to the expansion direction, reflecting that the average interparticle distance along the expansion direction is larger than that along the orthogonal direction. This behavior contrasts with the observations during slow compression. The measured aspect ratios are **B**) 1.34, **C**) 1.27, and **D**) 1.17 (with the trough area 76 %), which are significantly higher than those observed during slower compression, highlighting the pronounced anisotropy induced by the faster expansion process. Upon recompression, as the trough area decreases to 42 % (**Fig 4E-H**), the elongation direction shifts by 90° (**Fig 4E**), signifying that the average interparticle distance along the compression direction is shorter than that along the orthogonal direction. Then the intriguing 30° shift of the lattice orientation (“soft” to “hard” direction, **Fig 4G,H)** unfolds through a dynamic metastable phase transition (**Fig 4F**) with a rectangular (p2mm like) symmetry.

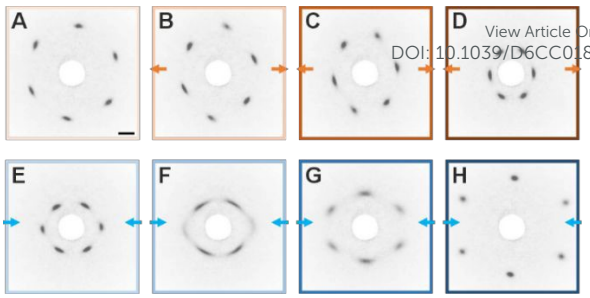

Figure 4. A rapid expansion-compression cycle of CS monolayer. **A**) 30 minutes after the compression of CS monolayer to approx. 30 mN/m (from **Figure 1**). **B**-**D**) Expansion (orange) and **E**-**H**) re-compression (blue) with barrier speed 27 mm/min. The scale bar corresponds to 10 mm.

Fig 5 depicts real space microstructures reconstructed from the diffraction patterns in **Fig 4**. Each panel includes an inset on the top right showing the corresponding Fast Fourier Transform (FFT) of the reconstructed microstructure, which agrees with the diffraction patterns shown in **Fig 4**. The Jupyter Notebook code used for the FFT generation can be found in **SI**. The reconstruction of real space microstructure was done using reciprocal lattice parameters acquired from the diffraction patterns: reciprocal lattice vectors (a^* and b^*) and the angle γ^* between them (see **Fig 2E**), to calculate the real space lattice vectors (a and b) and their corresponding angle γ, where $\gamma = 180° - \gamma^*$. The magnitudes of the real space vectors were determined based on the inverse proportionality between the reciprocal and real lattices ($a \propto 1/a^*$, $b \propto 1/b^*$). Operation of stretching and rotation (using an angle between the compression/expansion axis and a^*, see **Fig S3**) were applied independently to account for lattice deformations. The microstructure in **Fig 5A** exhibits an initial hexagonal arrangement, with a uniform distribution of particles (representing microgels at the air/water interface) and minimal deformation. As the expansion proceeds (**Fig 5B**-**D**), the particles along the expansion direction are further away from each other, decreasing the particle number density along the expansion direction. The simultaneous decrease in particle number density along the orthogonal direction (fixed width, w of the trough) suggests that the microgels also exhibit vertical mobility during the fast barrier movement. **Fig 5D**-**H** illustrate the behavior of the microgel monolayer during compression, showing a dynamic reorganization of the particles similar to what was observed in the expansion cycle, i.e., the reversible and adaptive nature of the microgel lattice. Moreover, the 30° shift of lattice orientation and the rectangular metastable phase captured as diffraction patterns in **Fig 4E**-**H**, and the corresponding reconstructed microstructure in **Fig 5D**-**G** bear a strong resemblance to the simulated FFTs and hexagonal array lateral compression in the “soft direction” in **Fig 3D-F** via a transitional phase with a rectangular symmetry. Across all simulations, microgels deform by sliding into neighboring rows, even when vertical rearrangement occurs. It is worth noting that in **Fig 5F**, despite the symmetry of the diffraction patterns resembling a rectangular lattice due to the fading pair of Bragg peaks along the compression axis, the reconstruction of the microstructure was based on hexagonal symmetry, as the diffraction pattern still exhibits six Bragg peaks. Consequently, the reconstruction accuracy in this case may be lower than the others, where the Bragg peaks are more distinct and well-defined.

Stopping the compression at the metastable rectangular phase results in immediate (matter of seconds) relaxation of the monolayer back into hexagonal symmetry, although reproducible over multiple compression and expansion cycles, see **Fig S4** and **Table S2**. Neither the conventional Langmuir-Blodgett deposition at a fixed Π nor the Langmuir-Schäfer deposition method was able to capture the induced metastable phase or the anisotropy of the microgel monolayers at the air/water interface on a substrate. This is likely due to the rearrangement of microgels during the drying process in the thin water film on the solid substrate, driven by immersion capillary forces.[19] Knowing the hexagonal lattice orientation and the stretching directions enables control over the deposition process, allowing for either linear or rectangular orders to be achieved on a solid substrate. Using our CS microgels, we successfully obtained non-hexagonal orders via reverse Langmuir-Blodgett deposition, see **Fig S5** and **S6**. Similar to the method described in ref,[29] the monolayer is deposited on hydrophobically surface-modified substrates from air to the subphase, i.e., water. Hydrophobic surface modification enhances the adhesion between the microgels and the substrate, effectively preventing the rearrangement of microgels in the thin water film.[30] Such rearrangement occurs when the monolayer is transferred onto a like-charged (as microgels) hydrophilic substrate from water to air, i.e., from below the monolayer at the air/water interface.[19] Several non-hexagonal orders of such monolayers on solid substrates (*ex situ*) were also reported for similarly sized coreless microgels,[8] hairy particles,[31] and binary systems.[32, 33]

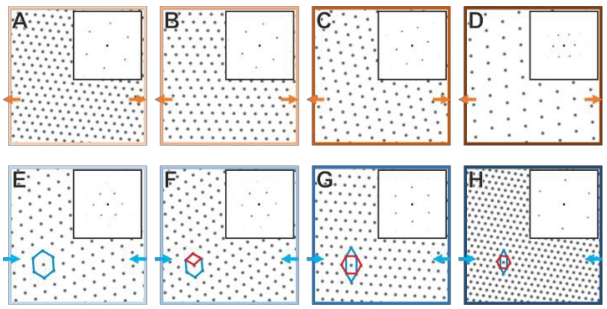

Figure 5. Reconstructed real space microstructure of the microgel monolayer during expansion (orange) and compression (blue), derived from the diffraction patterns in **Figure 4**. The insets in the top right display the corresponding fast Fourier transforms (FFTs) of each image.

In this work, we have studied the dynamic structural changes in CS microgel monolayers at air/water interfaces under uniaxial compression and expansion, captured in real time by small-angle light scattering. We demonstrate a reproducible 30° shift in hexagonal lattice orientation, mediated by a metastable rectangular phase. We attribute this behavior to the softness and deformability of microgels, which allow them to act simultaneously as individual building blocks and as an elastic sheet. This work captures the rich dynamic landscape accessible only through *in situ* observation. We hope this study inspires further investigations into the effects of confinement geometry (e.g., trough shape) on resulting microstructures, and the role of various shell morphologies.

Conflicts of interest

There are no conflicts to declare.

View Article Online
DOI: 10.1039/D6CC01855F

Data availability

All data generated or analyzed during this study are included in this published article (and its supplementary information files).

Author contribution

Acknowledgements

1. F. Bresme and M. Oettel, *Journal of Physics: Condensed Matter*, 2007, **19**, 413101.
2. E. Vignati, R. Piazza and T. P. Lockhart, *Langmuir*, 2003, **19**, 6650-6656.
3. M. He, J. P. Gales, É. Ducrot, Z. Gong, G.-R. Yi, S. Sacanna and D. J. Pine, *Nature*, 2020, **585**, 524-529.
4. I. T. Chen, E. Schappell, X. Zhang and C.-H. Chang, *Microsystems & Nanoengineering*, 2020, **6**, 22.
5. Y. Fang, B. M. Phillips, K. Askar, B. Choi, P. Jiang and B. Jiang, *Journal of Materials Chemistry C*, 2013, **1**, 6031.
6. D. M. Balazs, T. A. Dunbar, D.-M. Smilgies and T. Hanrath, *Langmuir*, 2020, **36**, 6106-6115.
7. S. Mičky, M. Bodík, M. Mičetić, F. Fetzer, M. Strienz, V. Held, M. Jergel, A. Schnepf, F. Schreiber and P. Šiffalovič, *Langmuir*, 2022, **38**, 14850-14856.
8. M. A. Fernandez-Rodriguez, M.-N. Antonopoulou and L. Isa, *Soft Matter*, 2021, **17**, 335-340.
9. M. J. Bergman, N. Gnan, M. Obiols-Rabasa, J.-M. Meijer, L. Rovigatti, E. Zaccarelli and P. Schurtenberger, *Nature Communications*, 2018, **9**, 5039.
10. S. Bochenek, C. E. McNamee, M. Kappl, H.-J. Butt and W. Richtering, *Physical Chemistry Chemical Physics*, 2021, **23**, 16754-16766.
11. D. Feller and M. Karg, *Soft Matter*, 2022, **18**, 6301-6312.
12. E. Guzmán and A. Maestro, *Polymers*, 2022, **14**, 1133.
13. S. Ciarella, M. Rey, J. Harrer, N. Holstein, M. Ickler, H. Löwen, N. Vogel and L. M. C. Janssen, *Langmuir*, 2021, **37**, 5364-5375.
14. M. Rey, M. A. Fernandez-Rodriguez, M. Karg, L. Isa and N. Vogel, *Accounts of Chemical Research*, 2020, **53**, 414-424.
15. E. A. Jagla, *Physical Review E*, 1998, **58**, 1478-1486.
16. K. Kuk, V. Abgarjan, L. Gregel, Y. Zhou, V. Carrasco Fadanelli, I. Buttinoni and M. Karg, *Soft Matter*, 2023, **19**, 175-188.
17. T. Kawamoto, K. Yanagi, Y. Nishizawa, H. Minato and D. Suzuki, *Chemical Communications*, 2023, **59**, 13289-13292.
18. A. Rubio-Andrés, D. Bastos-González and M. A. Fernandez-Rodriguez, *Journal of Colloid and Interface Science*, 2025, **688**, 328-340.
19. K. Kuk, J. Ringling, K. Gräff, S. Hänsch, V. Carrasco-Fadanelli, A. A. Rudov, I. I. Potemkin, R. Von Klitzing, I. Buttinoni and M. Karg, *Advanced Science*, 2024, **11**, 2406977.
20. V. Abgarjan, K. Kuk, J. L. S. Garthe, T. L. Wigger and M. Karg, *Soft Matter*, 2025, **21**, 5030-5044.
21. D. Y. Zang, E. Rio, D. Langevin, B. Wei and B. P. Binks, *The European Physical Journal E*, 2010, **31**, 125-134.

View Article Online
DOI: 10.1039/D6CC01855F

22. S. R. Vora, B. Bognet, H. S. Patanwala, C. D. Young, S. Y. Chang, V. Daux and A. W. K. Ma, *Journal of Colloid and Interface Science*, 2018, **509**, 94-101.
23. Y. S. Tein, B. R. Thompson, C. Majkrzak, B. Maranville, D. Renggli, J. Vermant and N. J. Wagner, *Review of Scientific Instruments*, 2022, **93**, 093903.
24. P. Cicuta and E. M. Terentjev, *The European Physical Journal E*, 2005, **16**, 147-158.
25. K. Kuk, L. Gregel, V. Abgarjan, C. Croonenbrock, S. Hänsch and M. Karg, *Gels*, 2022, **8**, 516.
26. C. A. Schneider, W. S. Rasband and K. W. Eliceiri, *Nature Methods*, 2012, **9**, 671-675.
27. R. W. Perry, M. C. Holmes-Cerfon, M. P. Brenner and V. N. Manoharan, *Physical Review Letters*, 2015, **114**, 228301.
28. E. Aumaitre, D. Vella and P. Cicuta, *Soft Matter*, 2011, **7**.
29. M. E. J. Hummel, C. Stelling, B. A. F. Kopera, F. A. Nutz, M. Karg, M. Retsch and S. Förster, *Langmuir*, 2019, **35**, 973-979.
30. L. H. Alvarez, A. A. Rudov, R. A. Gumerov, P. Lenssen, U. Simon, I. I. Potemkin and D. Wöll, *Physical Chemistry Chemical Physics*, 2021, **23**, 4927-4934.
31. J. Menath, J. Eatson, R. Brilmayer, A. Andrieu-Brunsen, D. M. A. Buzza and N. Vogel, *Proceedings of the National Academy of Sciences*, 2021, **118**, e2113394118.
32. M. Rey, A. D. Law, D. M. A. Buzza and N. Vogel, *Journal of the American Chemical Society*, 2017, **139**, 17464-17473.
33. F. Grillo, M. A. Fernandez-Rodriguez, M.-N. Antonopoulou, D. Gerber and L. Isa, *Nature*, 2020, **582**, 219-224.

All data generated or analysed during this study are included in this published article (and its supplementary information files).

View Article Online
DOI: 10.1039/D6CC01855F